

# A DEEP LEARNING MODEL FOR NUCLEAR MASS CLASSIFICATION OF PRIMARY COSMIC RAY INDUCED AIR SHOWERS BASED ON OBSERVABLE PARAMETERS

COSMINA MIHOREANU<sup>1,a</sup>, TUDOR ALEXANDRU CALAFETEANU<sup>1,b</sup>, PAULA GINA  
ISAR<sup>2,c,\*</sup>, EMIL IOAN SLUSANSCHI<sup>1,d</sup>

<sup>1</sup>Faculty of Automatic Control and Computer Science, National University of Science and Technology  
Politehnica Bucharest, Bucharest, Romania

<sup>a</sup>*cosmina.mihoreanu@stud.acs.upb.ro*, <sup>b</sup>*tudor.calafeteanu@upb.ro*, <sup>d</sup>*emil.slusanschi@upb.ro*

<sup>2</sup>Institute of Space Science - Subsidiary of INFLPR, Magurele, Ilfov, Romania

\*Corresponding author: *c.gina.isar@spacescience.ro*

*Compiled September 26, 2025*

Ultra-high-energy cosmic rays are still some of the most mysterious phenomena in astroparticle physics. Boasting energy levels of above 1 EeV ( $10^{18}$  eV), far higher than other particles traveling the Universe, or energies reached in the laboratory, they incite significant unanswered questions concerning their actual origin and nature. Highly energetic cosmic particles are a window into the study of fundamental physics at its limits and beyond. The most comprehensive method of studying them is by observing their signatures resulted from the atmospheric interactions in the developing extensive air shower (EAS). An EAS consists of secondary elementary particles produced in a cascade reaction from a primary cosmic ray particle entering the Earth's atmosphere. It can be traced on the ground using the powerful grid of radio detectors of the upgraded Pierre Auger Observatory (AugerPrime). The radio footprint of cosmic ray induced air shower events is fed to a convolutional neural network, alongside geometric characteristics extracted from CORSIKA 7 (with the CoREAS option) simulated air showers. Thus, modified ResNet and EfficientNet deep learning models are trained to classify the nuclear mass of the primary cosmic ray particle based on the observable parameters, with performances assessed by standard metrics such as Accuracy, F1 Score and MCC Score, which are shown to fluctuate, as expected, with the number and types of primary particles represented in the dataset, and the features included in the analysis, indicating the depth of the shower's maximum aperture ( $X_{\max}$ ) as the most valuable for the classification task, and the radio footprint image as a good replacement for the numerical simulation data. The classification metrics indicate an overall moderate positive rate, with accuracies of up to 83% reached for groups of particles with larger nuclear mass differences.

*Key words:* convolutional neural network, machine learning, cosmic rays, radio imaging.

*PACS:* 01.30.-y, 01.30.Ww, 01.30.Xx

## 1. INTRODUCTION

Ultra-high-energy cosmic rays (UHECRs) are subatomic particles that travel astronomical distances in the Universe at relativistic speeds, close to the speed of light. Most cosmic ray particles that reach our living planet Earth are protons (about 89%), followed by nuclei of the lightest elements, such as helium (10%), and only about 1% represent heavier nuclei, going up to iron or even uranium. The flux of UHECRs that reach energies above  $10^{18}$  eV is very low [1], and decreases with increased primary energy of cosmic rays, reaching the order of less than one particle per  $\text{km}^2$  per year. UHECRs are of great interest in the field of astroparticle physics, since their actual source origin and nature are still unknown [2], and more statistics and mass-sensitive measurements are needed to elucidate them.

The acceleration mechanisms of electrically charged particles with ultra-high energies, known to be of extragalactic origin [3], are not fully understood yet, since tracing their trajectories back towards the origin source, i.e., the ultimate laboratory in high-energy physics, faces several challenges, such as deflections in extragalactic magnetic fields. Tremendous efforts are put into the study of both the propagation of UHECRs with, e.g., advanced simulation frameworks like CRPropa [4], and the cosmic ray induced air showers modeled numerically with, e.g., the traditional CORSIKA simulation software [5], widely used in the scientific community.

The research frontier in UHECRs could provide new insights in the field of fundamental physics, from the point of view of hadronic interactions at ultra-high energy in developing air showers and thus elucidate, for example, the muon puzzler, i.e., the deficit of muons in simulations [6]. When a primary cosmic ray particle, e.g., a proton enters the Earth's atmosphere, it interacts with air molecules and develops into an avalanching cascade of billions of secondary elementary particles, such as photons, electrons, and muons (Figure 1).

Large-scale cosmic ray experiments are deployed to measure signals from air showers in different media, such as air, on the surface of the ground and under the ground. The Pierre Auger Observatory, the world's largest cosmic ray experiment, employs different detection techniques to indirectly measure UHECRs through induced air showers. It has been recording data since 2004 and, after over 20 years of operation [7], has currently started a new run of data taking with upgraded detectors [8] for ten more years, up until 2035. Its main detection techniques involve the water Cherenkov detectors (WCD) [9], i.e., 1660 in total with a maximum spacing of 1500 m, covering a surface area of  $3000 \text{ km}^2$ , and the fluorescence detectors (FD) [10], i.e., 27 in total, grouped at four different locations at the periphery of the experiment, overlooking the entire array. Observables like  $X_{\text{max}}$  [11], i.e., the atmospheric height of the maximum development of the air shower, estimated by the FD, and the muon number, recorded on the ground by the WCD [12], are the main air

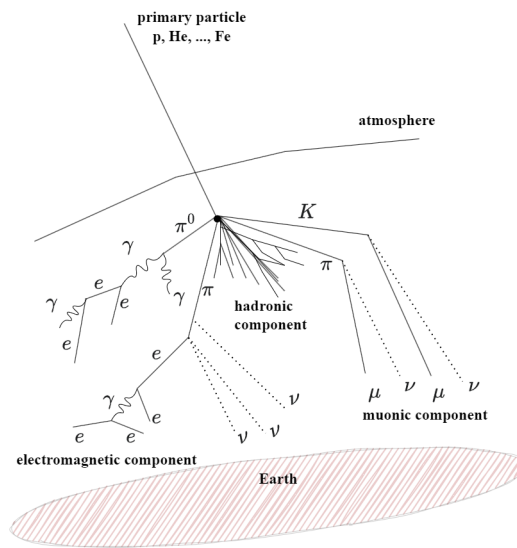


Fig. 1 – Illustration of a developing air shower with its main components [13].

shower variables used to estimate the nuclear mass of the primary cosmic ray. In the upgraded phase of the Observatory, the so-called AugerPrime, additional components are installed atop each WCD, such as a scintillator detector and a radio detector (RD) for mass-sensitive measurements and increased experiment exposure. The need for RD was previously proved by the Auger Engineering Radio Array (AERA), showing the importance of the radio detection technique as a complementary method in estimating the main shower observables [14], such as the energy and mass of the primary cosmic ray, and the direction of the incoming air shower. Moreover, AERA has found that the radio detection technique is highly sensitive to measuring highly inclined air showers with large footprints on the ground [15], which paved the way for the large-scale radio detector in the AugerPrime framework.

## 2. DEEP-LEARNING

As the volume of data collected by large-scale experiments increases with new upgrades, the need for automated processing methods rises. In past years, there have been studies leveraging the computing power of deep learning for the study of UHE-CRs, including an extensive study on the possibility of inferring  $X_{\max}$  and the mass composition using surface detector data from the Pierre Auger Observatory [11, 12].

Data analysis techniques applied on recorded cosmic ray events and simulations aid in the understanding of complex data in a relatively short time. Not only

can numeric observable characteristics of cosmic ray events be used to train shallow or deep learning models, but the radio footprints captured on the ground with radio detectors can be translated into 2D images to train image recognition models.

Convolutional neural networks (CNNs), well equipped to handle large volumes of data, are feed-forward networks distinguished by their convolutional layers of computation based on filter kernels. Neurons are spread out in a 3D structure, to account for the dimensions of the input data, and they work on the same principle of computing outputs and recalculating weights throughout the learning process.

Residual networks are a specific type of CNN, which works by bypassing parts of the architecture to prevent learning instability. A residual network, or ResNet, essentially works by adding skip connections to a regular neural network architecture, linking layers that are further away, and thus creating blocks that allow learning gradients to back-propagate faster during the training process [16]. Considering that image data is complex and often large-scale, it usually requires deeper networks, which can be more efficient and lead to better results when using a residual model, with shorter training times and higher accuracy [16].

Other widely used deep networks for image recognition tasks come from the EfficientNet family, an optimization of residual networks. An EfficientNet network uses a similar block-based architecture that enables fast training and a novel compound coefficient that is used to scale all relevant dimensions of the model in tandem, keeping a constant ratio, compared to an earlier model which scales up by independently manipulating the depth, width, and resolution of the network [17].

### 3. FRAMEWORK AND DATASET

Our framework [13] uses air shower simulations produced with CORSIKA 7 [5], with the CoREAS option (CORSIKA based Radio Emission from Air Showers) [18]. Simulations for this study are attributed to the Pierre Auger Collaboration, and they represent four different types of primary cosmic ray particles: proton (p), helium (He), nitrogen (N), and iron (Fe) nuclei. This current iteration is an extension of the previous dataset with two new primary particles (He and N), with nuclear masses still contained within the limits of p and Fe. Simulations are performed for a fixed shower core in the center of the Pierre Auger ideal detector map, i.e., with no gaps in the detector layout, where each point in the grid also denotes a radio antenna in the frame of AugerPrime RD. The simulated primary particles as shown in Figure 2 have zenith angles between 65 and 85 degrees (representing inclined air showers), a full range of azimuth angle (from 0 to 360 degrees), and a primary energy range from 2.5 to 119.5 EeV. About 2000 events are simulated for proton and nitrogen, while about 1000 events are simulated for helium and iron, with a total of 6256 events.

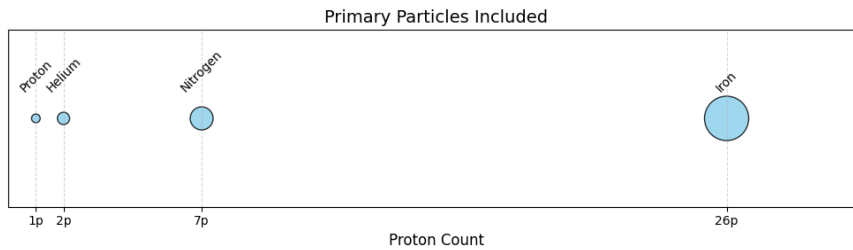


Fig. 2 – Mass differences between primary particles represented to scale.

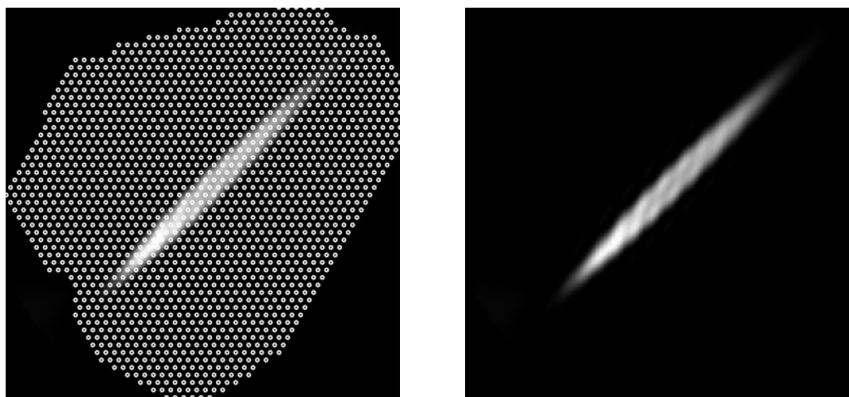


Fig. 3 – The interpolation of energy fluence over the ideal Auger map with (left) and without (right) antennas [13]. The white dots represent the surface particle detectors of the Pierre Auger Observatory.

The electric field strength of the registered radio signal in a time series gives the energy fluence, i.e., the measure of the energy lateral distribution over the unit area. The energy fluence distributions were transformed into a more straightforward visual representation of an event, by generating grayscale footprint images that represent the intensity of the energy fluence over the Pierre Auger ideal detector map (Figure 3), i.e., an interpolation on a 400x400 grid [13].

In addition to the four previous numerical features of the air shower ( $X_{\max}$ , energy, zenith, azimuth), an additional mass-sensitive input was included in the numerical dataset, i.e., the number of muons detected on the ground. As shown in Figure 4, the most effective numerical indicators of mass composition are  $X_{\max}$  and muon count [11, 12].

To further deepen the understanding of cosmic ray radiation patterns, we also extended the image dataset by generating images of the energy fluence distribution for each of the three polarization directions (east-west, north-south, vertical) of the radio signal from air showers, besides their total amplitude as used previously [13].

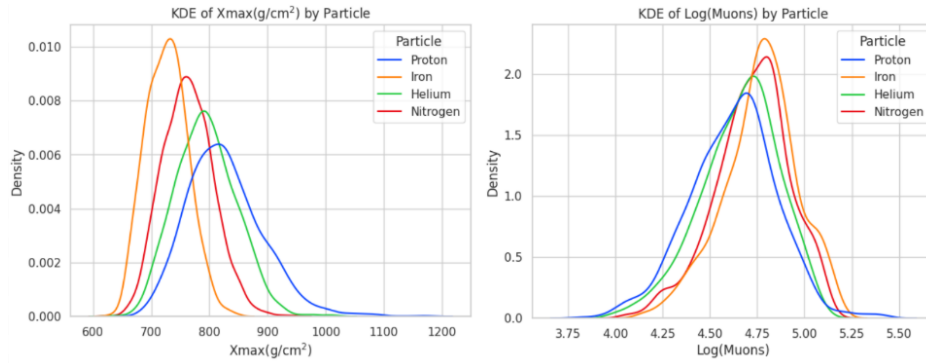


Fig. 4 – Distribution of  $X_{\max}$  (left) and  $\log(\mu\text{ons})$  (right) for all primary particle datasets.

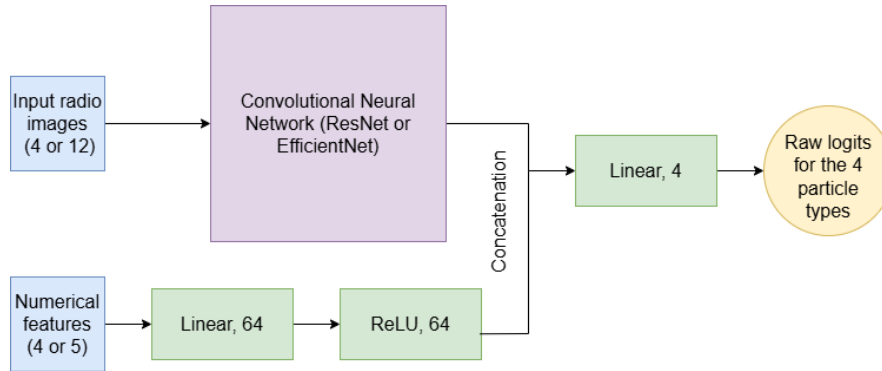


Fig. 5 – Neural Network Architecture.

The generalized architecture of the proposed neural network is shown in Figure 5. The radio images pass through a ResNet or EfficientNet convolutional neural network, with the first convolutional layer and the last classifier layer modified to accept more than three input channels, and output only a preliminary result that could merge with the result from a linear layer processing the numerical characteristics ( $X_{\max}$ , energy, zenith, azimuth, muon count). The images included for one event are either four in the original case or 12 when separating the polarizations.

#### 4. RESULTS

Previously [13], it was demonstrated that characteristics such as  $X_{\max}$  and the radio footprint of a cosmic ray induced air shower are good differentiators between protons and iron nuclei even on a small training and testing dataset of around 3000 events. Currently, we use additional datasets and characteristics of both shower de-

velopment and the corresponding radio signal strength to classify primary particles with varying performance.

Metrics by epoch for the entire dataset, in the case of using EfficientNet-B0 as a CNN block, show a final score of about 0.65 for Accuracy as seen in Figure 6. From Figure 7, with the test error rates per primary particle, including the train and overall test error of about 40%, it is clearly seen that the test error for helium is much higher than for the rest of the primaries, mainly due to the fact that helium is closer to the proton (in terms of mass composition) and is therefore often incorrectly classified as a proton instead of helium. Also, because of an unbalanced dataset, a lower error of about 20% is seen for proton and nitrogen (both primaries having the highest comparable number of events), compared to iron, showing an increased error due to a decreased number of events (same for helium).

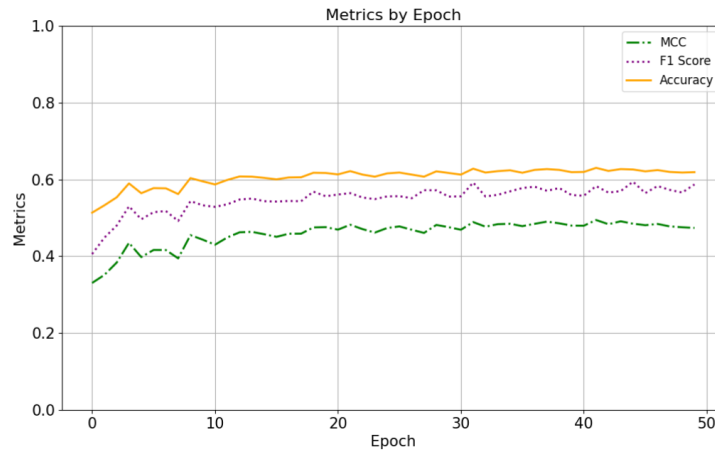


Fig. 6 – MCC, F1 score and Accuracy for 50 epochs on the entire four-particle dataset, using EfficientNet, muon counts and polarizations.

More runs of the algorithms were performed on the entire four-particle dataset, using three different CNN blocks, with progressively increasing depths and complexity: ResNet18, ResNet50 and EfficientNet-B0. A summary of our results is listed in Table 1, showing the values to which the standard metrics relevant for a classification task, MCC (Matthews Correlation Coefficient),  $F_1$ -score and Accuracy, converge after a number of 50 epochs. We conclude that the addition of separated polarizations does not add significant improvements to the performance, while the number of muons proves to be more relevant. Deeper models like ResNet50 and EfficientNet-B0 also provide slightly better results and stability.

In Table 2, we recorded the relevant metrics obtained when training the model on a number of subsets of particles taken from the entire dataset, also compared with

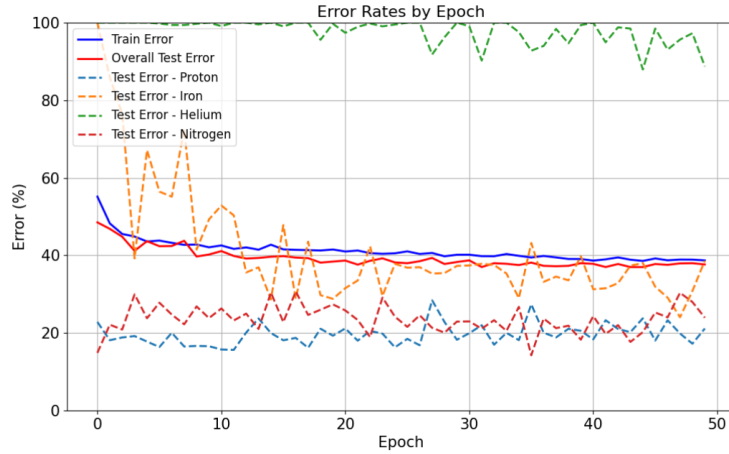


Fig. 7 – Train and test errors for all four particles, using EfficientNet, muon counts and polarizations.

Table 1.

Model performance metrics for all four primary particles (p, He, N, Fe).

Muons	Pols	Model	MCC	F <sub>1</sub> score	Accuracy
yes	yes	ResNet18	0.42	0.57	0.6
yes	yes	ResNet50	0.49	0.59	0.62
yes	yes	EfficientNet	0.48	0.59	0.62
yes	no	ResNet18	0.45	0.57	0.6
yes	no	ResNet50	0.48	0.58	0.61
yes	no	EfficientNet	0.49	0.59	0.62
no	yes	ResNet18	0.38	0.5	0.55
no	yes	ResNet50	0.39	0.5	0.55
no	yes	EfficientNet	0.4	0.51	0.56

the previous results for the proton-iron pair [13]. The low MCC for the proton-helium pair confirms the instability in the dataset, as the number of proton induced events is almost double that of helium events, while removing helium from the analysis levels up the MCC from 0.28 to 0.47 for the proton-iron-nitrogen group. The best results remain those obtained for pairs with higher mass composition differences, such as the ones including iron.

## 5. CONCLUSIONS

The purpose of this work was to expand the functionality of our analysis framework with additional input for the machine learning application designed to predict

Table 2.

Metrics for subsets of particle datasets, obtained with ResNet18.

Particles	MCC	F <sub>1</sub> score	Accuracy
p-Fe (old)	0.82	0.91	0.91
p-He-N-Fe	0.28	0.45	0.47
p-He	0.18	0.60	0.61
p-N	0.57	0.79	0.79
Fe-N	0.50	0.79	0.79
Fe-He	0.76	0.83	0.83
p-N-Fe	0.47	0.66	0.66

the type of primary cosmic ray particle, based on the observable characteristics of the extensive air shower. As a deep learning model can learn the patterns of air shower footprints and predict the mass composition of new incoming particles, it could give new insights into the nature and origin of cosmic rays.

The input dataset was updated with simulation libraries for two new primary particles (helium and nitrogen), with similar distributions of geometries and energies to those of the previous study. Two other features were introduced to predict the type of primary cosmic ray: the muon count and the polarizations of the radio signal. For each simulation, the field strength values of the recorded radio signal from air showers, per polarization, were translated into grayscale maps depicting the radiation intensity. These images and the numerical characteristics of each simulated event constituted the training data for a deep convolutional neural network that outputs a label corresponding to one of the four types of particles represented in the dataset.

The obtained results only showed slight, insignificant increases in the prediction accuracy, on the one hand due to the limited range of primary nuclei included, with fairly similar proton numbers, and on the other hand due to the size limitations of the dataset. Therefore, we consider that more statistics are needed for such a study, with simulation time being the only constraint for highly energetic air showers. As this study is a first-order approach and research forward, the main development direction was to test several different model configurations and options for the input data and explore their shortcomings, to be able to further optimize the framework. High-performance computing, and moreover, CORSIKA simulations with the MPI option, would highly contribute to speeding up calculations of large data volumes.

*Acknowledgements.* We thank the Pierre Auger Collaboration for the simulation libraries used in this study. This work was partially supported by the Romanian Ministry of Research, Innovation and Digitalization, under the Romanian National Core Program LAPLAS VII - contract no. 30N/2023.

## REFERENCES

1. A. Abreu et al., The Pierre Auger Collaboration, *The energy spectrum of cosmic rays beyond the turn-down around  $10^{17}$  eV as measured with the surface detector of the Pierre Auger Observatory*, Eur. Phys. J. C **81**, 966 (2021).
2. A. A. Halim et al., The Pierre Auger Collaboration, *Constraints on metastable superheavy dark matter coupled to sterile neutrinos with the Pierre Auger Observatory*, Phys. Rev. D **109**, L081101 (2024).
3. A. Aab et al., The Pierre Auger Collaboration, *Observation of a large-scale anisotropy in the arrival directions of cosmic rays above  $8 \times 10^{18}$  eV*, Science **357**, 1266–1270 (2017).
4. R. A. Batista et al., *CRPropa 3.2 – an advanced framework for high-energy particle propagation in extragalactic and galactic spaces*, J. Cosmol. Astropart. Phys. **09**, 035 (2022).
5. D. Heck, J. Knapp, J. N. Capdevielle, G. Schatz, T. Thouw et al., *Corsika: A monte carlo code to simulate extensive air showers*, Report FZKA **6019**, 11 (1998).
6. A. A. Halim et al., The Pierre Auger Collaboration, *Testing hadronic-model predictions of depth of maximum of air-shower profiles and ground-particle signals using hybrid data of the Pierre Auger Observatory*, Phys. Rev. D **109**, 102001 (2024).
7. A. A. Halim et al., The Pierre Auger Collaboration, *Large-scale Cosmic-ray Anisotropies with 19 yr of Data from the Pierre Auger Observatory*, Astrophys. J. **976**, 49 (2024).
8. A. A. Halim et al., The Pierre Auger Collaboration, *The Pierre Auger Observatory and its Upgrade*, Science Reviews - from the end of the world (Argentina) **1**, 8–33 (2020).
9. J. Abraham et al., The Pierre Auger Collaboration, *The Pierre Auger Cosmic Ray Observatory*, Nucl. Instrum. Methods Phys. Res. Sec. A **798**, 172–213 (2015).
10. The Pierre Auger Collaboration, *The fluorescence detector of the Pierre Auger Observatory*, Nucl. Instrum. Methods Phys. Res. Sec. A **620**, 227–251 (2010).
11. A. A. Halim et al., The Pierre Auger Collaboration, *Measurement of the depth of maximum of air-shower profiles with energies between  $10^{18.5}$  and  $10^{20}$  eV using the surface detector of the Pierre Auger Observatory and deep learning*, Phys. Rev. D **111**, 022003 (2025).
12. A. A. Halim et al., The Pierre Auger Collaboration, *Inference of the mass composition of cosmic rays with energies from  $10^{18.5}$  to  $10^{20}$  eV using the Pierre Auger Observatory and deep learning*, Phys. Rev. Lett. **134**, 021001 (2025).
13. T. A. Calafeteanu, P. G. Isar, and E. I. Slușanschi, *Convolutional neural network processing of radio emission for nuclear composition classification of ultrahigh-energy cosmic rays*, Universe **10**, 327 (2024).
14. A. A. Halim et al., The Pierre Auger Collaboration, *Radio measurements of the depth of air-shower maximum at the Pierre Auger Observatory*, Phys. Rev. D **109**, 022002 (2024).
15. A. Aab et al., The Pierre Auger Collaboration, *Observation of inclined EeV air showers with the radio detector of the Pierre Auger Observatory*, J. Cosmol. Astropart. Phys. **10**, 026 (2018).
16. M. Tan and Q. Le, *Efficientnet: Rethinking model scaling for convolutional neural networks*, Proceedings of the 36th International Conference on Machine Learning, PMLR **97**, 6105–6114 (2019).
17. M. S. Ebrahimi and H. K. Abadi, *Study of residual networks for image recognition*, In Intelligent Computing: Proceedings of the 2021 Computing Conference **2**, 754–763 (2021).
18. T. Huege, M. Ludwig, C. W. James, *Simulating radio emission from air showers with CoREAS*, AIP Conference Proceedings **1535**, 128–132 (2013).